Article

LABEL-FREE OPTICAL BIOSENSORS BASED ON APTAMER-FUNCTIONALIZED POROUS SILICON SCAFFOLDS

Katharina Urmann, Johanna Gabriela Walter, Thomas Scheper, and Ester Segal

Anal. Chem., **Just Accepted Manuscript** • DOI: 10.1021/ac504487g • Publication Date (Web): 30 Dec 2014

LABEL-FREE OPTICAL BIOSENSORS BASED ON APTAMER-FUNCTIONALIZED POROUS SILICON SCAFFOLDS

*Katharina Urmann[1,2], Johanna-Gabriela Walter[1], Thomas Scheper[1], Ester Segal[2]**

[1] Institute for Technical Chemistry, Leibniz University of Hannover, Callinstr. 5, 30167 Hannover, Germany

[2] Department of Biotechnology and Food Engineering, Technion Israel Institute of Technology, Technion City, 32000 Haifa, Israel; phone: +972-4-8295071; e-mail: esegal@tx.technion.ac.il

KEYWORDS

Optical Biosensor, Aptamer, Porous Silicon, Label-Free, Protein Detection

ABSTRACT

A proof-of-concept for a label-free and reagentless optical biosensing platform based on nanostructured porous silicon (PSi) and aptamers is presented in this work. Aptamers are oligonucleotides (single-stranded DNA or RNA) that can bind their targets with high affinity and specificity, making them excellent recognition elements for biosensor design. Here we describe the fabrication and characterization of aptamer-conjugated PSi biosensors, where a previously characterized his-tag binding aptamer (6H7) is used as model system. Exposure of the aptamer-functionalized PSi to the target proteins as well as to complex fluids (i.e., bacteria lysates containing target proteins), results in robust and well-defined changes in the PSi optical interference spectrum, ascribed to specific aptamer-protein binding events occurring within the nano-scale pores, monitored in real time. The biosensors show exceptional stability and can be easily regenerated by a short rinsing step for multiple biosensing analyses. This proof-of-concept study demonstrates the possibility of designing highly stable and specific label-free optical PSi biosensors, employing aptamers as capture probes, holding immense potential for application in detection of a broad range of targets, in a simple yet reliable manner.

INTRODUCTION

Since the establishment in 1990 of an *in vitro* selection process for short, single-stranded oligonucleotides with a desired target affinity, these molecules are referred to as aptamers [1,2], and have emerged as promising capture probes for biosensing applications. Aptamers can be designed to capture virtually any desired target, e.g. whole cells, proteins and small molecules [3], by using the SELEX (Systematic Evolution of Ligands by Exponential Enrichment) process for their synthesis. When used as receptor molecules, these synthetic oligonucleotides present significant advantages compared to antibodies, while easily accessible in high and constant quality [3]. Aptamers exhibit exceptional stability, their small size facilitates high surface coverage, and their ability for reversible folding enables the design of sensitive yet regenerable biosensing schemes [3,4]. Aptamers were already selected for many different targets including ions, small organic molecules (dyes, amino acids, ATP, vitamins, antibiotics, several drugs), peptides, proteins, cells or microorganisms and the catalogue is steadily growing [3,5,6]. In addition to this diversity in targets, aptamers can be modified during their synthesis either on 5' or 3' terminus of the oligonucleotide to introduce functional groups, which allow their facile immobilization onto a variety of surfaces [7].

Over the past decade, aptamer-based biosensors, also called aptasensors, have been extensively developed, presenting an immense potential to replace traditional antibody-based assays, due to their high sensitivity and stability [4,5,8-11]. Additionally, their unique selection process opens up the possibility to target substances that do not have alternative specific receptors available, emphasizing their suitability as a receptor element for biosensing.

Various aptasensor schemes are reported in the literature, ranging from label-dependent methods such as electrochemistry, fluorescence and chemiluminescence [12-14] to label-free optical methods,

which are mainly limited to surface plasmon resonance (SPR) [15-19]. SPR is inarguably a well-established and highly sensitive method; nevertheless, a particular challenge in SPR application is the limited sensor area, leading to a diminished capacity [20]. In addition, SPR-based transducers are particularly sensitive to ambient temperature drift and, for maximal performance this parameter must be controlled, making the instrumentation complex and expensive [21]. Thus, SPR analysis requires highly skilled-personnel and is mostly confined to a laboratory setting.

In recent years, porous silicon (PSi) has emerged as a promising nanomaterial for the design of different optical label-free biosensing platforms, owing to its large surface area, versatile chemistry and straightforward fabrication [22-35]. PSi-based interferometers, in which a change in refractive index of the solution contained within the porous nanostructure can be measured, are most common and the technique is often referred to as reflective interferometric Fourier transform spectroscopy (RIFTS) [30,33,36,37]. Briefly, the reflectivity spectrum of a PSi sensor is comprised of a series of Fabry-Perot interference fringes resulting from reflections at the top and bottom interfaces of the porous thin film. The position of the peak along the x-axis in the RIFTS spectrum corresponds to the effective optical thickness (EOT), which equals $2nL$ (where n is the effective refractive index and L is the physical thickness of the porous layer). Changes in n or L, lead to proportional shifts in the reflectivity spectra and therefore in the EOT value [38]. Thus, the biosensing concept relies on monitoring changes in the EOT of PSi with a conjugated capture probe as a response to target binding. So far, PSi-based biosensors have employed only conventional receptor molecules, such as antibodies or enzymes [33,39-42].

Herein, we describe, for the first time, the design and characterization of a label-free optical PSi-based aptasensor. An oxidized porous silicon nanostructure (Fabry-Pérot thin film), used as the optical transducer, is conjugated with a well-characterized his-tag binding aptamer (6H7) [43-45].

This aptamer system has been previously used for protein purification processes and was thoroughly investigated in microarray applications as described by Walter *et al.* [46]. We confirm successful immobilization of the aptamer throughout the oxidized PSi ($PSiO_2$) scaffold by attenuated total reflectance Fourier transform infrared (ATR-FTIR) spectroscopy and confocal microscopy. Aptamer-protein binding events, occurring within the nano-scale pores, are monitored in real time, confirming affinity of the aptamer-immobilized $PSiO_2$ towards the target proteins in μM range as anticipated by this specific aptamer binding characteristics [43]. The high selectivity and specificity of this biosensing scheme is demonstrated also in complex biological fluids such as bacteria lysates. Furthermore, as the aptamer is engineered to withstand repeated cycles of denaturation and renaturation, the biosensor exhibits outstanding stability and reusability for numerous subsequent experiments.

EXPERIMENTAL SECTION

Materials. Highly doped p-type Si wafers (0.0008 Ω·cm resistivity, <100>-oriented, B-doped) were purchased from Siltronix Corp. Aqueous HF (48%) and ethanol absolute were supplied by Merck. (3-aminopropyl)triethoxysilane (APTES), *N*-(3-Dimethylaminopropyl)-*N*-ethylcarbodiimide hydrochloride (EDC), succinic acid and all buffer salts were purchased from Sigma-Aldrich Chemicals. All solutions were prepared with Milli-Q water (18.2 MΩ cm) and filtered prior to use. Anti-his-tag aptamer 6H7 (5'- GCT ATG GGT GGT CTG GTT GGG ATT GGC CCC GGG AGC TGG C - 3') sequence was taken from the US patent specification U.S.7329742 (Doyle and Murphy, 2008). 6H7 was selected in 50 mM K_2HPO_4, 150 mM NaCl, 0.05% Tween 20 (this buffer composition is subsequently abbreviated as PBS-T). As Tween 20 is known to be responsible for partial blocking of amino-modified surfaces, immobilization and

washing steps, as well as renaturation of the aptamer were carried out in PBS-T without Tween 20 (abbreviated as PBS). Aptamers were purchased with a 5'-amino modification from BioSpring (Frankfurt, Germany). Additional aptamers with 5'-amino modification as well as 3'-Cy5 fluorescent dye for laser confocal microscopy imaging were purchased from Integrated DNA Technologies (Coralville, USA). Proteins for biosensing experiments included casein, IgG (Sigma-Aldrich Chemicals) and 6xhis T6 lipase from *Geobacillus stearothermophilus,* referred to as lipase, generously supplied by Prof. Ayelet Fishman. As a negative control, *Escherichia coli* strain JL-102 was cultured in Luria broth (LB) medium (10 g/L casein peptone, 10 g/L NaCl, 5 g/L yeast extract, all purchased from Sigma-Aldrich Chemicals).

Preparation of Bacteria and their Lysates. A shaking flask with 20 ml sterile LB medium was inoculated with 100 µl of a freeze culture of *E. coli* JL-102 (free of plasmids) and cultured over night, shaking at 37°C. The resulting culture was used for biosensing experiments to mimic a biologically relevant complex fluid.

2 ml of bacteria culture were spun down in a standard lab centrifuge, replacing the supernatant by 1 ml PBS selection buffer. Following the re-suspension, the culture was ultrasonicated at 4°C (Labsonic M, Sartorius Stedim Biotech, Göttingen, Germany). Following removal of cell debris, the suspension was centrifuged again and the supernatant taken to a fresh tube and further used as the bacteria lysate.

Preparation of Oxidized PSi. Si wafers (single side polished, <100> oriented and heavily doped, p-type) were electrochemically etched in a 3:1 (v/v) solution of aqueous HF (48%) and ethanol for 30 s at a constant current density of 300 mA/cm^2. CAUTION: HF is a highly corrosive liquid, and it has to be handled with extreme care and under secured working conditions! Si wafers with an exposed area of 1.33 cm^2 were contacted on the back side with a

strip of aluminum foil and mounted in a Teflon etching cell; a Platinum mesh was used as the counter electrode. After etching, the surface of the wafer was rinsed with ethanol several times and dried under dry nitrogen gas flow. The freshly etched PSi samples were thermally oxidized in a tube furnace (Thermolyne) at 800°C for 1 h in ambient air resulting in oxidized PSi ($PSiO_2$) scaffolds.

Scanning Electron Microscopy. High-resolution scanning electron microscopy (HRSEM) of the neat $PSiO_2$ scaffold was performed using a Carl Zeiss Ultra Plus HRSEM with an accelerating voltage of 1 keV.

Characterization of $PSiO_2$ Films. The structural properties, i.e., thickness and porosity, of the $PSiO_2$ layers were characterized by HRSEM, gravimetry (for porosity), and SLIM (spectroscopic liquid infiltration method) methods, as we previously described [47]. Detailed description regarding the application of gravimetry and SLIM for the characterization of PSi nanomaterials can be found elsewhere [48]. Spectroscopic ellipsometry measurements of the neat $PSiO_2$ scaffold were carried out with a Woolam M-2000 UI Ellipsometer. Measurements were fitted with an effective medium approximation.

Functionalization of $PSiO_2$ Films. The $PSiO_2$ samples were incubated with a solution of 42 mM APTES in toluene for 1 h. After the solution was removed, the surface was rinsed with toluene, ethanol and acetone and dried under a nitrogen stream. The APTES-modified surface was then immersed in a freshly prepared solution of 100 mg succinic acid in 4.7 ml DMSO and 300 µl of 0.1 M $NaHCO_3$, pH 9.4 for 30 min. After removal of the solution, the surface was washed extensively with DMSO two times and with purified water.

In order to follow the reflectivity changes upon the surface modifications, the sample was mounted in a custom made Plexiglas flow cell and fixed underneath the light source. An O-ring

inside the cell limits the modified area and an in- and outlet allow the injection of solutions for the different reaction steps (see Table 1). Table 1 summarizes the detailed procedure followed for the biosensor preparation. Briefly, a 52 mM EDC solution was injected to the flow cell and allowed to react for 1 h. Subsequently, 50 µl of 75 µM aptamer solution were applied to the sensor for 1 h, followed by thorough washing with 10 ml of 50 mM Tris buffer and a final folding of the aptamer by incubation in PBS for 30 min.

Table 1. Synthetic steps followed for aptamer immobilization onto $PSiO_2$ and details of protein biosensing experiment.

Reaction step	Details	Volume	Incubation time
Washing/Wetting	PBS	10 ml	*
EDC activation	52 mM EDC in PBS	1 ml	1 h
Aptamer immobilization	75 µM aptamer in PBS	50 µl	1 h
Washing	50 mM Tris buffer	10 ml	*
Elution	PBS-T, 1 M imidazole	10 ml	30 min
Aptamer folding	PBS	10 ml	30 min
Sensing	Protein diluted in PBS-T	50 µl	1 h
Washing	PBS	10 ml	*
Readout	PBS	10 ml	30 min
Elution	PBS-T, 1 M imidazole	10 ml	30 min
Regeneration	PBS	10 ml	30 min

* indicates that the sensor is gently rinsed in a time interval of 2 min

Measurement of Interferometric Reflectance Spectra. Interferometric reflectance spectra of the samples were collected using an Ocean Optics charge-coupled device (CCD) USB 4000 spectrometer fitted with a microscope objective lens coupled to a bifurcated fiber-optic cable. A tungsten light source was focused onto the center of the sample surface with a spot size of

approximately 1-2 mm^2. Reflectivity data were continuously recorded every 15 s in the wavelength range of 400-1000 nm, with a spectral acquisition time of 100 ms. Both, illumination of the surface and detection of the reflected light were performed along an axis coincident with the surface normal. All the optical experiments were conducted in a fixed cell to ensure that the sample reflectivity is measured at the same spot during all measurements. Spectra were collected using a CCD spectrometer and analyzed by applying fast Fourier transformation (FFT), as previously described by Massad-Ivanir *et al.* [49]. Figure S-1 (see Supporting Information) depicts representative reflectivity spectra of the $PSiO_2$ nanostructure before and after binding of the target molecules, as well as the fast Fourier transformation (FFT) of the reflectivity spectra, leading to a single peak, whose position (corresponds to the value of *2nL*, EOT) was monitored. In the present work, the data is presented as relative EOT and defined as:

$$EOT/EOT_0 = \left(\frac{EOT_{readout}}{EOT_{at\ baseline}}\right)$$

Please note that the term EOT_0 refers to the averaged EOT obtained during baseline establishment at the beginning of the optical experiments.

Infrared Spectroscopy. Surface modification was verified using attenuated total reflectance Fourier transform infrared (ATR-FTIR) spectroscopy. Spectra were recorded using a Thermo 6700 FTIR instrument equipped with a Smart iTR diamond ATR device.

Protein Biosensing. Biosensing experiments were carried out in a flow cell configuration, described for the functionalization of $PSiO_2$ scaffolds, immediately following the preparation of the biosensor. The aptamer-functionalized $PSiO_2$ samples were incubated with the protein solution (in PBS-T) for 1 h. After removal of the protein solution and flushing the cell with PBS, the sample was incubated for 30 min in PBS (see Table 1). For the regeneration of the biosensor,

the protein was eluted with 1 M imidazole, followed by the renaturation of aptamers in PBS (see Table 1). Optical measurements were recorded every 15 s throughout the whole experiment. Please note that during buffer exchange and rinsing steps, EOT measurements were shortly paused for to allow a thorough washing of the biosensor and the flow cell.

Confocal Laser Microscopy. For confocal microscopy studies samples were scanned immediately after sensor functionalization, using a Cy5-labeled aptamer for immobilization. A LSM 700 confocal laser-scanning microscope (Carl Zeiss, Inc.) linked to a Zeiss inverted microscope equipped with a Zeiss X63 oil immersion objective was utilized. Laser lines of 405 nm were irradiated for the excitation of the $PSiO_2$ structure. Signals for $PSiO_2$ and the Cy5-labeled aptamers were obtained at 420 nm and 635 nm, respectively. For three-dimensional image projection of the porous structure, z-scans in 0.35 μm increments were taken over a depth of ~10 μm and projected by using standard Carl Zeiss software (ZEN 2009).

RESULTS AND DISCUSSION

Functionalization of $PSiO_2$ films with amino-modified aptamers. The PSi films were prepared from a highly doped p-type crystalline Si wafer by an electrochemical etching process at 300 mA/cm^2 for 30 s. The resulting freshly-etched PSi film was then thermally oxidized at 800°C to create a hydrophilic $PSiO_2$ scaffold [38]. The average values for scaffold characterization are summarized in Table S-1 (see Supporting Information). Briefly, the resulting porous layers are around 5400 nm thick and the calculated porosity is approximately 80%. The SLIM results are in excellent agreement with spectroscopic ellipsometry experiments, in which fitting with the effective medium approximation, results in a calculated layer thickness of 5000 nm and porosity

of 79%. HRSEM studies (top-view and cross-section) of the films reveal their highly porous nature and depict interconnecting cylindrical pores ranging in diameter from 50 to 80 nm (see Figure S-2, Supporting Information). It should be noted that the resulting nanostructure is characterized by a high specific surface area and porous volume over a small working area (980 cm^2 STP cm^{-2} and $3.24x10^{-4}$ cm^3 STP cm^{-2} [50], respectively with STP being standard temperature and pressure), facilitating an effective large volume for monitoring reactions/events occurring within the pores.

The synthetic approach for grafting the amino-modified aptamers onto the $PSiO_2$ surfaces is based on well-established silanization and coupling chemistries, which we have previously employed for conjugation of single-stranded DNA onto PSi nanostructures [39]. The detailed synthesis scheme is outlined in Scheme 1. First, the $PSiO_2$ film was treated with APTES in toluene, resulting in an amino-silanized surface (Scheme 1-I). In the following step, the amino groups were capped by succinic anhydride, forming a carboxylated surface (Scheme 1-II). Finally, the amine-terminated oligonucleotide was conjugated via EDC coupling chemistry (Scheme 1-III-IV), resulting in an aptamer-functionalized $PSiO_2$.

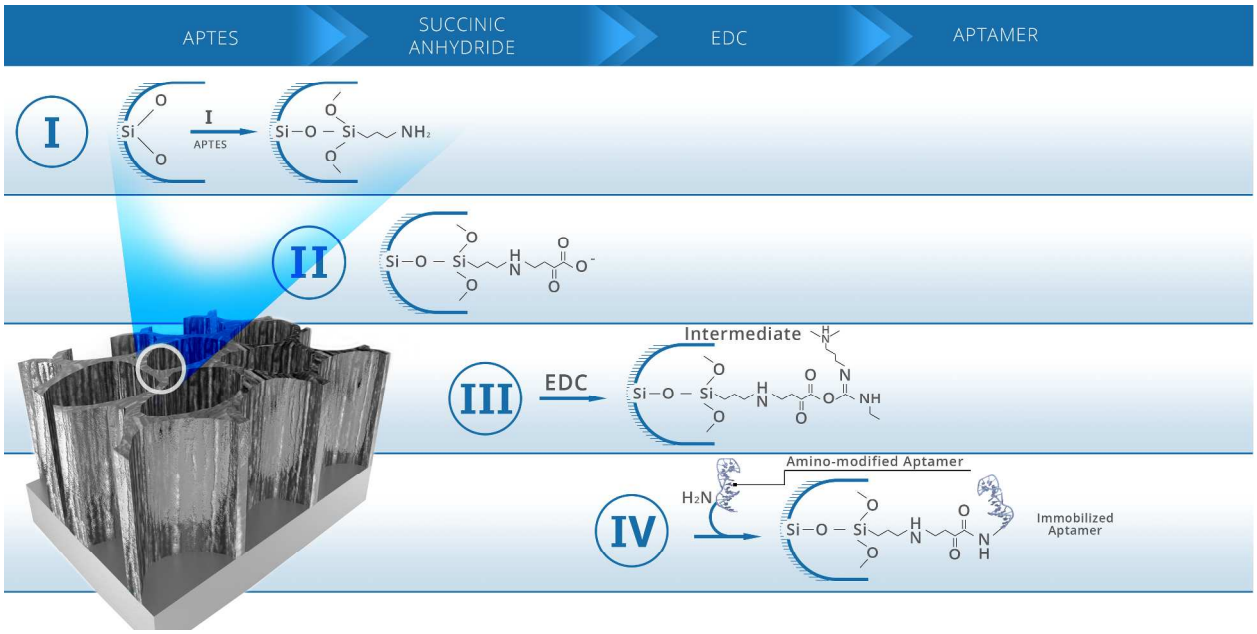

Scheme 1. Surface modification and immobilization steps. (I) Silanization of the $PSiO_2$ surface. (II) Carboxylation and (III) EDC-induced formation of the active intermediate (INT). (IV) Covalent binding of the amino-modified aptamer.

To confirm the immobilization of the aptamer to the $PSiO_2$ scaffold, samples were characterized using ATR-FTIR spectroscopy. Figure 1(a) shows the ATR-FTIR spectra of the porous film following the different modification steps. The spectrum of the neat $PSiO_2$ surface shows a typical $-(O_ySiH_x)$ vibration mode at 801 cm^{-1} and a peak at 1039 cm^{-1} that is related to the Si-O-Si stretching mode. The APTES-modified surface spectrum (Fig. 1a-I) depicts two additional peaks; the 1641 cm^{-1} is ascribed to the bending of primary amine and the 1555 cm^{-1} to the bending of protonated amines [51]. Following the modification with succinic anhydride, the spectrum shows two strong bands near 1400 and 1570 cm^{-1} for the symmetric and the antisymmetric stretching vibration, respectively, indicative of the deprotonated carboxylate group (Fig. 1a-II) [52,53]. Characteristic DNA bands, around 1688 cm^{-1} (carbonyl), as well as around 1230 cm^{-1} (phosphate groups), are observed after conjugation of the aptamer (Fig. 1a-IV). As a control, the neat $PSiO_2$ was incubated with the 6H7 aptamer solution under similar conditions, followed for aptamer conjugation, and washed with PBS prior to FTIR analysis. The resulting spectrum (Fig. 1a, control trace) shows minor changes in comparison to the neat $PSiO_2$, which may be ascribed to electrostatic interaction of the negatively charged-aptamer and highly-porous film [3,54].

Immobilization onto the PSi nanostructure was also validated by confocal laser microscopy imaging using an aptamer sequence with a Cy5-dye conjugated to its 3' end. Figure 1(b) depicts z-stack images of $PSiO_2$ films with two different aptamer concentrations (30 and 100 μM). These

images reveal that the aptamer was immobilized both on the top surface and throughout the entire porous scaffold. Using low and high aptamer concentrations, results in significant differences in the fluorescence signal intensity, ascribed to different surface coverage values. For the subsequent biosensing experiments, we used an intermediate aptamer concentration of 75 μM. It is crucial for target recognition, that the aptamers maintain their ability to fold in their specific 3D-structure; thus, based on our preliminary results (data not shown) an intermediate aptamer concentration was employed to provide sufficient surface coverage by the aptamers yet allowing spacing for folding and target recognition [55,56]. In line with these findings and to ensure a high yield of functional aptamers, we have introduced an additional step of aptamer unfolding (in elution buffer) and refolding (in PBS) following the aptamer conjugation to the PSi scaffold (see Table 1).

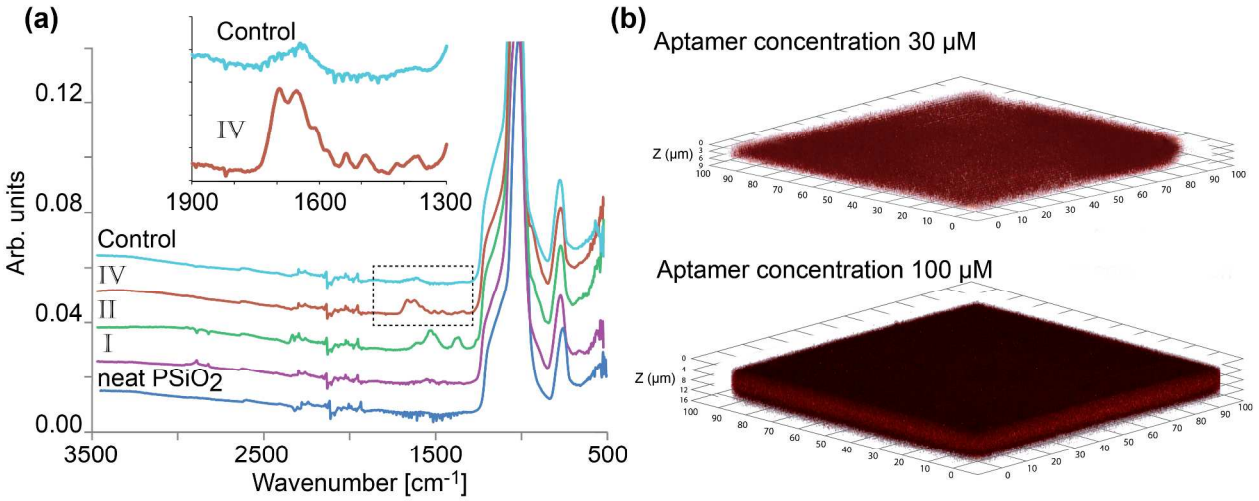

Figure 1. (a) ATR-FTIR of the different functionalization steps (illustrated in Scheme 1) followed for the preparation of aptamer-immobilized $PSiO_2$: (I) APTES-modified surface; (II) Succinic anhydride-modified surface and (IV) 6H7-modified surface. As a control, neat $PSiO_2$

was incubated with the 6H7 aptamer solution under similar conditions and washed with PBS. **(b)** Confocal microscope z-stack images of $PSiO_2$ sensors conjugated with different aptamer-concentrations (30 μm and 100 μm of Cy5-labeled 6H7 aptamer).

Optical biosensing experiments. As a model system we chose the 6H7 aptamer [43], which is designed to target the polyhistidine tag (his-tag) of proteins. In our previous work we have thoroughly characterized this aptamer and demonstrated its binding affinity to his-tagged proteins [45,46]. A typical dissociation constant (calculated from the Langmuir isotherm) of 4.6 μM was determined for the aptamer when immobilized onto magnetic particles [43]. To investigate the potential of the 6H7-functionalized $PSiO_2$ for biosensing, we have studied its optical response to a variety of his-tagged (6x His) protein targets, characterized by different properties and molecular weights. In a typical biosensing experiment, the 6H7-functionalized $PSiO_2$ is exposed to a solution containing the target protein and the reflectivity spectra of the porous film is monitored in real time and corresponding EOT values are computed. Figure 2 presents the change in the relative EOT values (EOT/EOT_0) upon exposure of the 6H7-functionalized $PSiO_2$ to lipase (T6 from *Geobacillus stearothermophilus*, molecular weight 44 kDa) at a concentration of 19 μM. First, PBS buffer was introduced into the flow cell to acquire a stable EOT baseline. Following this step, the lipase solution was introduced and the sample was incubated with the solution. Immediately after the introduction of the lipase, a rapid increase in the relative EOT value was observed, after which the signal steadily increased until a constant EOT value was attained (after ~ 1 h). The increase in the EOT is attributed to the infiltration of the protein solution into the pores and to binding events of the his-tagged protein to the 6H7 aptamer. Next, the protein solution was removed and the biosensor surface extensively rinsed with PBS (during

this washing step, EOT acquisition was briefly paused). Subsequently, due to removal of the unbound protein molecules, the relative EOT sharply decreased and a stable EOT value was obtained, corresponding to a net EOT shift of 40 nm. This significant EOT shift is attributed to binding of the target protein to the aptamer-functionalized surface. The stability of the EOT signal during the rinsing step implies that the captured protein molecules are tightly bound to the aptamer under these conditions. It should be emphasized that exposure of the biosensor to non his-tagged proteins e.g, casein and human IgG, did not induce significant changes in the relative EOT (see Figure S-3, Supporting Information). This clearly indicates that the developed surface chemistry protocol in combination with the high surface coverage by the aptamers, provide an effective passivation of the sensor surface and minimize effects of non-specific binding.

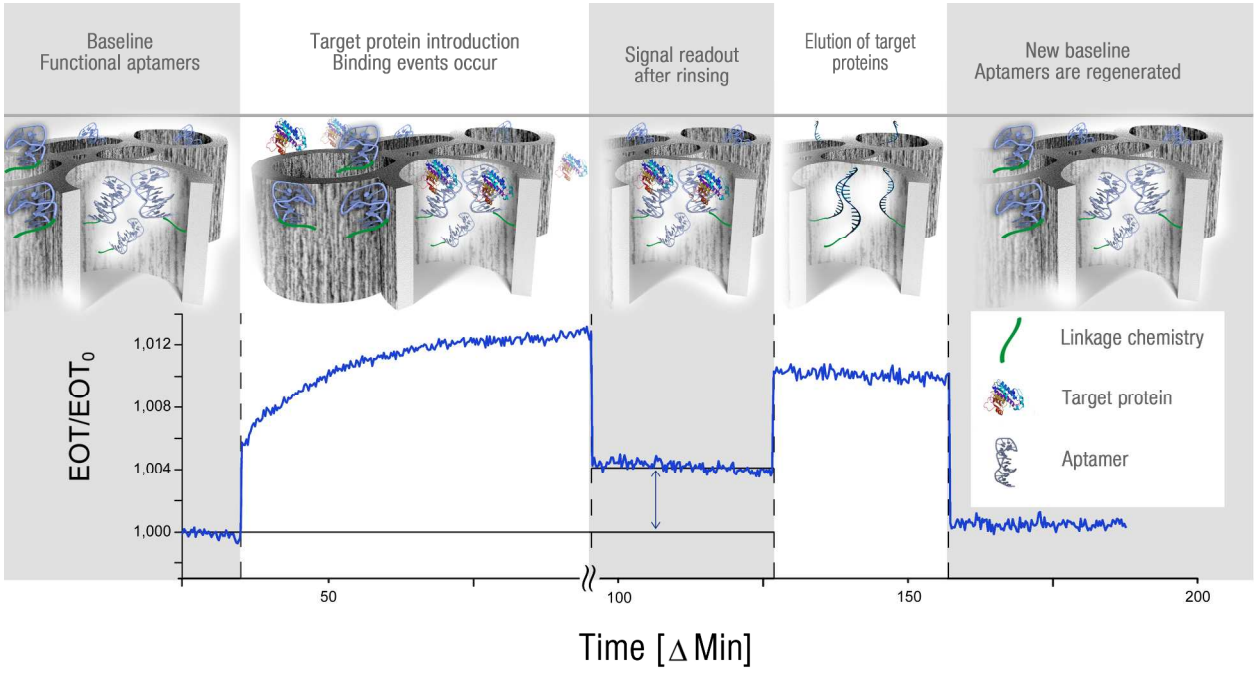

Figure 2. Relative EOT value vs. time of 6H7-functionalized $PSiO_2$ during a typical biosensing experiment. A baseline is obtained in buffer solution followed by the introduction of lipase

solution, binding events occur and the signal increases rapidly. After a rinse step to remove unbound molecules, a stable readout signal is attained. Competitive elution with 1 M imidazole leads to the release of the captured target protein and the rapid removal of such in the following rinse step. Following a short incubation in the aptamer's selection buffer, the biosensor can be restored for subsequent use. Note that during buffer exchange and rinsing, EOT measurements are briefly paused.

One of the main advantages of aptamers over conventional recognition elements (e.g., antibodies) is their ability to undergo reversible changes of conformation with variations in temperature or salt concentration, rendering aptamer-based sensors as potentially recyclable [57]. Alternatively, gentle elution conditions can be pre-defined during SELEX to facilitate aptamer regeneration during application processes [58]. In case of the aptamer 6H7, we have eluted the target protein by exposing the biosensor to a high concentration of imidazole (a strong chelating agent) see Figure 2. This results in an immediate increase in EOT signal (corresponding to a net shift of approximately 120 nm) due to the higher refractive index of this buffer solution (n=1.347). This elution procedure was adapted from immobilized metal ion affinity chromatography (IMAC), which is conventionally used for the purification of His-tagged proteins [44]. Whereas, imidazole is the most common and effective agent for elution and recovery of captured His-tagged proteins from an IMAC column [59]. Indeed, following this step, the relative EOT readout returns to its original value. Figure 2 demonstrates that we were able to remove the captured proteins from the biosensor surface. Consequently, the biosensors were incubated with PBS. Following this step, the biosensor was exposed to the lipase solution for subsequent optical experiments. Figure 3 depicts the optical response of the biosensor, expressed

in terms of the relative EOT shift, upon consecutive exposure to different protein solutions. The biosensor exhibited highly reproducible results i.e., similar EOT shifts were obtained during cycling of lipase solution (28 μM). Whereas, upon subsequent exposure of the biosensor to a high concentration solution of a non-target protein i.e., casein (78 μM), no EOT shift was observed, demonstrating the high specificity of this biosensing platform. Furthermore, successive introduction of target/non-target protein mixtures, containing lipase and casein (at a concentration of 28 μM and 39 μM, respectively), resulted in reproducible EOT shifts, corresponding to the concentration of the lipase target. It should be noted that all these experiments were carried out using a single biosensor, demonstrating the stability of our biosensing scheme and the ability to reuse the biosensor for numerous subsequent experiments. Figure S-4 (see Supporting Information) presents the relative EOT vs. time data for these experiments, and details how data was extracted for Figure 3.

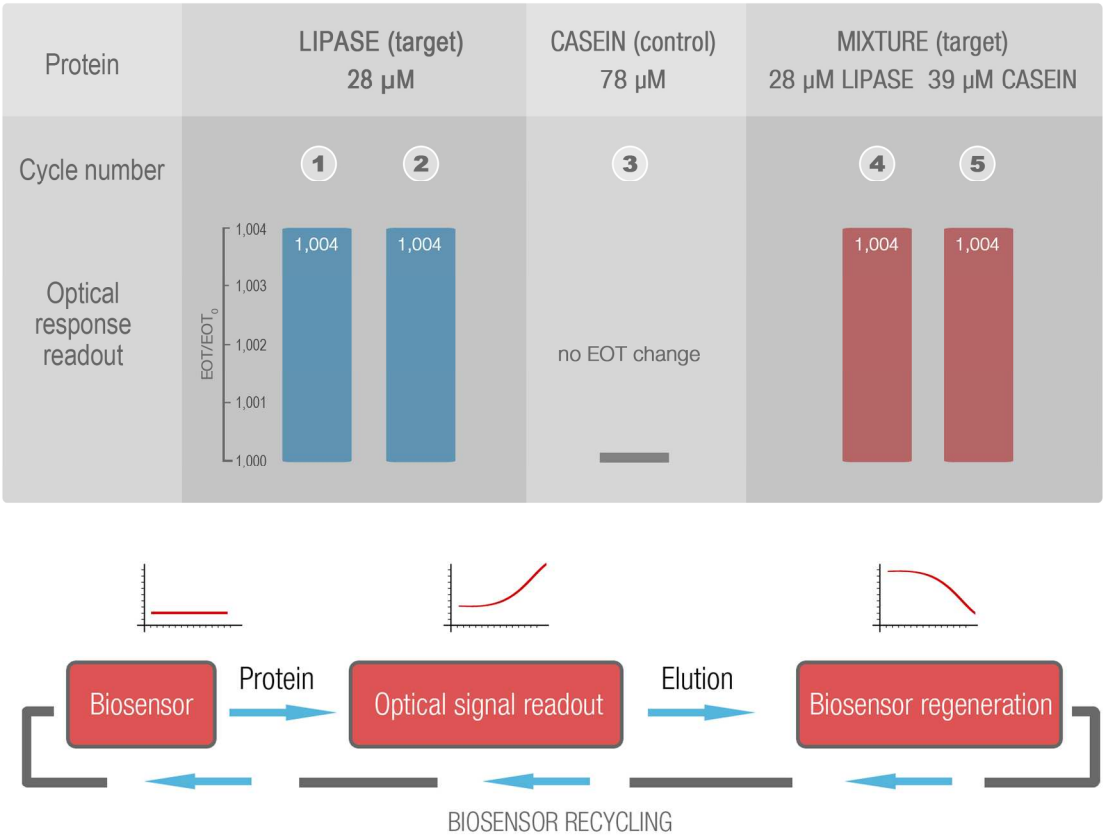

Figure 3. Biosensing results, expressed in terms of the averaged relative EOT value, for the 6H7-functionalized $PSiO_2$ exposed to 28 µM lipase for two subsequent cycles (cycle 1 and 2); a successive third cycle of exposure to 78 µM casein (cycle 3, used as a negative control). Consequently, the biosensor was exposed to a protein mixture, containing 28 µM lipase and 39 µM casein, for two additional cycles (cycles 4 and 5). All experiments were carried out on a single biosensor sample. Schematics underneath depict the course of biosensing experiments and the mode of biosensor regeneration and cycling. Figure S-4 (see Supporting Information) presents the relative EOT vs. time data for these experiments, and details how data was extracted.

A key challenge in PSi biosensors is to effectively stabilize the nanostructure during experiments in biological solutions, as PSi oxidation and dissolution in aqueous environments lead to significant signal baseline drifts, signal loss, and ultimately to structural collapse of the PSi thin film [25,40,60]. Also in the case of the aptamer-functionalized $PSiO_2$ biosensors, baseline drifts were observed during the prolonged exposure to buffer solutions (EOT/EOT_0 = 1,0040 after 4 h of buffer flow). Nevertheless, we were able to reuse the biosensors for numerous subsequent experimental cycles. The aptamer-functionalized $PSiO_2$ biosensor was used for subsequent 12 sensing cycles, showing their excellent reusability (see Table S-2). To the best of our knowledge, this is the first report on PSi-based optical affinity biosensors utilizing aptamers as capture probes, demonstrating their successful reuse while retaining detection accuracy, as presented in Figure 3. It should be noted that all experiments were carried out in solution and following the regeneration step (see Figure 3), the biosensor was dried under a stream of nitrogen and stored overnight. After usage of >7 days time period, the PSi film showed poor optical properties. Visual assessment of the biosensor suggested residues of salts and protein to have clogged the pores and therefore impaired its performance.

The dynamic range of the biosensor was studied by exposing the biosensor to a set of lipase solutions with different concentrations (0-56 μM). Figure 4 summarizes the results of these experiments, depicting the maximal relative EOT value attained for each protein concentration. All experiments were carried out using 6H7-functionalized $PSiO_2$ surface by performing biosensing experiments with varying lipase concentration. All experiments were performed in triplicates and IgG is introduced as a non-target protein control. Indeed, no optical shifts were observed upon exposure to IgG, demonstrating again the excellent selectivity of the 6H7

aptamer. A good linear correlation between the relative EOT signal and the protein concentration is obtained ($R^2 = 0.985$).

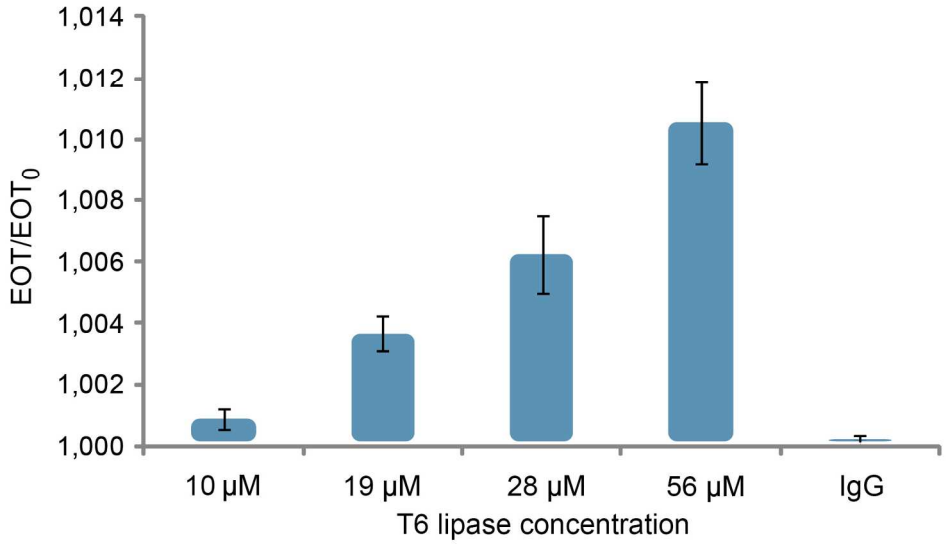

Figure 4. Optical response (relative EOT) of the biosensor vs. lipase concentration. The concentration row, including the negative control with IgG (non-target protein), was carried out on a single biosensor and repeated again on a different biosensor scaffold.

Biosensing in complex biological fluids. One of the major obstacles in the application of label-free biosensors is the ability to detect the target molecule in complex biological fluid in which it resides [61,62]. This is ascribed to the strong interference from non-specific binding of non-target proteins onto the transducer/solution interface [63]. Thus, to study the ability of our biosensor to selectively detect target molecules in the presence of overabundant non-specific proteins, the aptamer-immobilized $PSiO_2$ was exposed to an overnight bacterial culture grown in LB medium as well as to bacteria lysate solution, both are rich in overabundant non-specific proteins (but do not contain target his-tagged proteins). Figure 5 shows the optical response of the biosensor, expressed as the maximal relative EOT value attained, upon exposure to these complex

biological fluids. For the bacterial culture suspension, negligible EOT changes were observed; exposure to the bacteria lysate solution (total protein concentration is 1.8 mg/ml) induced a minor increase in the relative EOT value of 6 nm. These values are similar to those observed upon exposure to the biosensor to non-target protein solutions in buffer at protein concentrations corresponding to 2 mg/ml (see Fig. 3 and Fig. 4). On the other hand, introduction of the biosensor to a bacteria lysate solution, overexpressing target his-tagged proteins (total protein concentration is 19.6 mg/ml), resulted in a profound change in the relative EOT of 67 nm. Please note that experiments with pure lipase samples were conducted in concentrations of 0-56 μM, corresponding to a range of 0-2.47 mg/ml. These results demonstrate the ability of this biosensing platform to selectively detect its target protein in a complex solution of bacteria lysate. This is attributed to the excellent specificity of the 6H7 aptamer and to its viable immobilization strategy and surface modification, minimizing non-specific adsorption of unrelated molecules. Thus, when designing a PSi-based biosensor with other aptamer-target pairs, non-specific interactions between the capture probe, the modified surface, the appropriate target as well as possible interfering substances, must be carefully studied and optimized accordingly. This is critical when targeting proteins, as properties such as the isoelectric point, molecular weight and folding will affect both target recognition and unintended adsorption onto the biosensor [64].

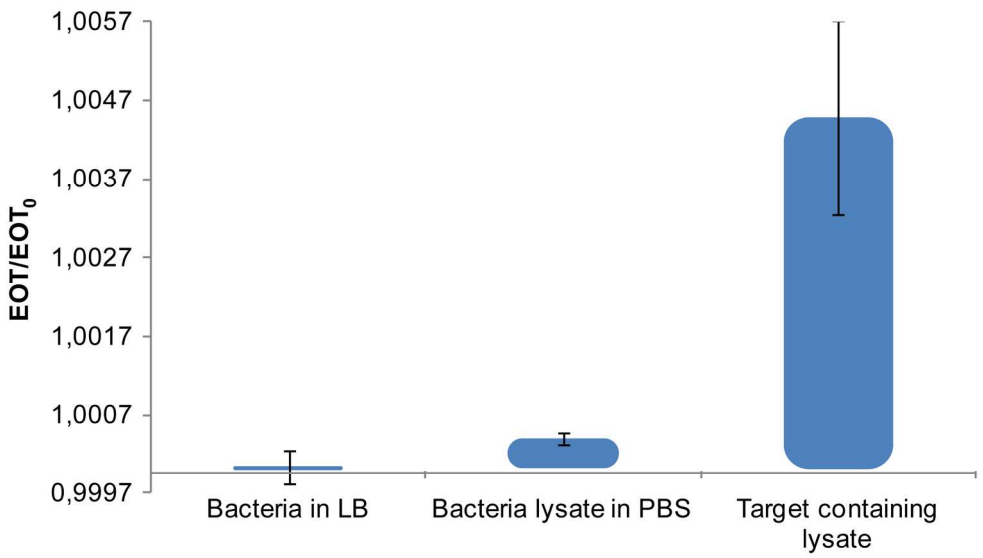

Figure 5. Optical response (relative EOT) of the biosensor to different complex fluids. A single biosensor was subsequently exposed to an overnight bacterial culture grown in LB medium, a solution of bacteria lysate in PBS, and a target-containing bacterial lysate solution.

Current work in our lab is focused on a few aspects: (i) reducing the overall analysis time by optimizing the assay; (ii) exploring the use of more sophisticated PSi structures such as rugate filters, to improve the sensor resolution and (iii) employment of aptamers with lower affinity constants to address the sensitivity aspect. We expect these advancements to result in biosensors exhibiting superior sensitivity according to the dissociation constant of the aptamers (i.e. in nanomolar range) and will make them indeed comparable to the performance of antibody-based PSi biosensors.

CONCLUSIONS

In this proof-of-concept work, a label-free optical biosensor based on aptamer-conjugated porous Si (Fabry-Perot layers) was designed and characterized. For the first time, a model aptamer was

covalently immobilized onto the oxidized PSi nanostructure and the resulting biosensor scheme demonstrated specific binding of target proteins, detected and quantified by RIFTS. Exposure to the target proteins, also in mixture solutions (containing target and non-target proteins) and even complex fluids (bacteria in culture media and their lysates), resulted in highly robust and reproducible changes in the optical reflectivity spectrum of the biosensor corresponding to the affinity constant of the used aptamer model system. Control experiments revealed negligible binding of non-target proteins, even in complex biological fluids, confirming the excellent selectivity of these aptamer-based biosensors towards their target analytes. Importantly, the biosensors show exceptional stability and could be easily regenerated by a short rinsing step for multiple biosensing analyses.

The presented optical label-free biosensor scheme holds a great promise for the design of versatile bioanalytical assays, allowing for rapid detection and quantification of analytes in a simple and reliable manner. The superior properties of aptamers as recognition elements, mainly their availability for various targets and their excellent selectivity and stability, combined with the advantages of PSi-optical transducers, can be exploited for construction of simple, flexible, inexpensive, robust and portable biosensing platforms. Where many biosensing schemes fail due to their lack of stability in real world samples and settings, the presented system can fill this gap and provide a real alternative to antibody-based assays.

ACKNOWLEDGMENT

We thank Prof. Ayelet Fishman and her PhD student, Adi Dror, from the Department for Biotechnology and Food Engineering, at the Technion - Israel Institute of Technology, for

supplying target proteins. We are grateful to Prof. Rolf Brendel and Sascha Wolter at the Institute for Solar Energy Research Hamelin, Germany, for performing the spectroscopic ellipsometry measurements. ES and KU acknowledge the core services and support from the Lorry I. Lokey Center for Life Science and Engineering.

SUPPORTING INFORMATION AVAILABLE

This information is available free of charge via the Internet at http://pubs.acs.org/.

REFERENCES

(1) Tuerk, C.; Gold, L. *Science* **1990**, *249*, 505-510.
(2) Ellington, A. D.; Szostak, J. W. *Nature* **1990**, *346*, 818-822.
(3) Song, S.; Wang, L.; Li, J.; Fan, C.; Zhao, J. *Trends in Analytical Chemistry* **2008**, *27*, 108-117.
(4) O'Sullivan, C. *Analytical and Bioanalytical Chemistry* **2002**, *372*, 44-48.
(5) Walter, J. G.; Heilkenbrinker, A.; Austerjost, J.; Timur, S.; Stahl, F.; Scheper, T. *Zeitschrift für Naturforschung B* **2012**, *67b*, 976-986.
(6) You, K.; Lee, S.; Im, A.; Lee, S. *BIOTECHNOL BIOPROC E* **2003**, *8*, 64-75.
(7) Lönne, M.; Zhu, G.; Stahl, F.; Walter, J.-G. In *Biosensors Based on Aptamers and Enzymes*, Gu, M. B.; Kim, H.-S., Eds.; Springer Berlin Heidelberg, 2014, pp 121-154.
(8) Famulok, M.; Mayer, G. *Acc Chem Res* **2011**, *44*, 1349-1358.
(9) Gu, M. B.; Kim, H.-S. *Biosensors Based on Aptamers and Enzymes*; Springer, 2014; Vol. 140, p 331.
(10) Sefah, K.; Phillips, J. A.; Xiong, X.; Meng, L.; Van Simaeys, D.; Chen, H.; Martin, J.; Tan, W. *The Analyst* **2009**, *134*, 1765-1775.
(11) Han, K.; Liang, Z.; Zhou, N. *Sensors* **2010**, *10*, 4541-4557.
(12) Cho, H.; Yeh, E.-C.; Sinha, R.; Laurence, T. A.; Bearinger, J. P.; Lee, L. P. *ACS Nano* **2012**, *6*, 7607-7614.
(13) Zhou, J.; Ellis, A. V.; Kobus, H.; Voelcker, N. H. *Analytica Chimica Acta* **2012**, *719*, 76-81.
(14) Giamberardino, A.; Labib, M.; Hassan, E. M.; Tetro, J. A.; Springthorpe, S.; Sattar, S. A.; Berezovski, M. V.; DeRosa, M. C. *PLoS ONE* **2013**, *8*, e79087.
(15) Kim, D. K.; Kerman, K.; Hiep, H. M.; Saito, M.; Yamamura, S.; Takamura, Y.; Kwon, Y. S.; Tamiya, E. *Analytical Biochemistry* **2008**, *379*, 1-7.
(16) Bai, H.; Wang, R.; Hargis, B.; Lu, H.; Li, Y. *Sensors (Basel, Switzerland)* **2012**, *12*, 12506-12518.
(17) Tombelli, S.; Minunni, M.; Luzi, E.; Mascini, M. *Bioelectrochemistry* **2005**, *67*, 135-141.
(18) Ashley, J.; Li, S. F. *Biosensors and Bioelectronics* **2013**, *48*, 126-131.
(19) Tran, D. T.; Knez, K.; Janssen, K. P.; Pollet, J.; Spasic, D.; Lammertyn, J. *Biosensors and Bioelectronics* **2013**, *43*, 245-251.
(20) Couture, M.; Zhao, S. S.; Masson, J.-F. *Physical Chemistry Chemical Physics* **2013**, *15*, 11190-11216.

(21) Leonard, P.; Hearty, S.; Brennan, J.; Dunne, L.; Quinn, J.; Chakraborty, T.; O'Kennedy, R. *Enzyme and Microbial Technology* **2003**, *32*, 3-13.
(22) De Stefano, L.; Arcari, P.; Lamberti, A.; Sanges, C.; Rotiroti, L.; Rea, I.; Rendina, I. *Sensors* **2007**, *7*, 214-221.
(23) Pacholski, C. *Sensors* **2013**, *13*, 4694-4713.
(24) Jane, A.; Dronov, R.; Hodges, A.; Voelcker, N. H. *Trends in Biotechnology* **2009**, *27*, 230-239.
(25) Kilian, K. A.; Bocking, T.; Gooding, J. J. *Chemical Communications* **2009**, *0*, 630-640.
(26) Alvarez, S. D.; Schwartz, M. P.; Migliori, B.; Rang, C. U.; Chao, L.; Sailor, M. J. *physica status solidi (a)* **2007**, *204*, 1439-1443.
(27) Dancil, K.-P. S.; Greiner, D. P.; Sailor, M. J. *Journal of the American Chemical Society* **1999**, *121*, 7925-7930.
(28) Janshoff, A.; Dancil, K. P. S.; Steinem, C.; Greiner, D. P.; Lin, V. S. Y.; Gurtner, C.; Motesharei, K.; Sailor, M. J.; Ghadiri, M. R. *Journal of the American Chemical Society* **1998**, *120*, 12108-12116.
(29) Orosco, M. M.; Pacholski, C.; Miskelly, G. M.; Sailor, M. J. *Adv. Mater.* **2006**, *18*, 1393-1396.
(30) Pacholski, C.; Yu, C.; Miskelly, G. M.; Godin, D.; Sailor, M. J. *Journal of the American Chemical Society* **2006**, *128*, 4250-4252.
(31) Schwartz, M. P.; Derfus, A. M.; Alvarez, S. D.; Bhatia, S. N.; Sailor, M. J. *Langmuir* **2006**, *22*, 7084-7090.
(32) Schwartz, M. P.; Alvarez, S. D.; Sailor, M. J. *Analytical Chemistry* **2006**, *79*, 327-334.
(33) Gaur, G.; Koktysh, D.; Weiss, S. M., 2013, pp 859408-859408-859411.
(34) Zhang, J.; Wu, Y.; Zhang, B.; Li, M.; Jia, S.; Jiang, S.; Zhou, H.; Zhang, Y.; Zhang, C.; Turner, A. P. F. *Analytical Letters* **2012**, *45*, 986-992.
(35) Gupta, B.; Zhu, Y.; Guan, B.; Reece, P. J.; Gooding, J. J. *The Analyst* **2013**, *138*, 3593-3615.
(36) Tsang, C. K.; Kelly, T. L.; Sailor, M. J.; Li, Y. Y. *ACS Nano* **2012**, *6*, 10546-10554.
(37) Pacholski, C.; Sartor, M.; Sailor, M. J.; Cunin, F.; Miskelly, G. M. *Journal of the American Chemical Society* **2005**, *127*, 11636-11645.
(38) Segal, E.; Perelman, L. A.; Cunin, F.; Di Renzo, F.; Devoisselle, J. M.; Li, Y. Y.; Sailor, M. J. *Advanced Functional Materials* **2007**, *17*, 1153-1162.
(39) Shtenberg, G.; Massad-Ivanir, N.; Moscovitz, O.; Engin, S.; Sharon, M.; Fruk, L.; Segal, E. *Analytical Chemistry* **2012**, *85*, 1951-1956.
(40) Massad-Ivanir, N.; Shtenberg, G.; Segal, E. *Advances in Experimental Medicine and Biology* **2012**, *733*, 37-45.
(41) Bonanno, L. M.; DeLouise, L. A. *Biosensors and Bioelectronics* **2007**, *23*, 444-448.
(42) Krismastuti, F. S. H.; Pace, S.; Voelcker, N. H. *Advanced Functional Materials* **2014**, *24*, 3639-3650.
(43) Kökpinar, Ö.; Walter, J.-G.; Shoham, Y.; Stahl, F.; Scheper, T. *Biotechnology and Bioengineering* **2011**, *108*, 2371-2379.
(44) Doyle, S. A.; Murphy, M. B. *US Patent 0142582 A1* **2005**.
(45) Zhu, G.; Lübbecke, M.; Walter, J.; Stahl, F.; Scheper, T. *Chemical engineering & technology* **2011**, *34*, 2022-2028.
(46) Walter, J. G.; Kökpinar, O.; Friehs, K.; Stahl, F.; Scheper, T. *Analytical Chemistry* **2008**, *80*, 7372 - 7378.

(47) Massad-Ivanir, N.; Shtenberg, G.; Zeidman, T.; Segal, E. *Advanced Functional Materials* **2010**, *20*, 2269-2277.
(48) Sailor, M. J. *Porous Silicon in Practice*; Wiley-VCH: Weinheim, 2011, p 250.
(49) Massad-Ivanir, N.; Shtenberg, G.; Tzur, A.; Krepker, M. A.; Segal, E. *Analytical Chemistry* **2011**, *83*, 3282-3289.
(50) Massad-Ivanir, N.; Friedman, T.; Tzur-Balter , A.; Nahor, A.; Eichler, S.; Bonanno, L. M.; Sa'ar, A.; Segal, E. *Soft Matter* **2012**, *8*, 9166-9176.
(51) Shtenberg, G.; Massad-Ivanir, N.; Fruk, L.; Segal, E. *ACS Applied Materials & Interfaces* **2014**, *6*, 16049-16055.
(52) Barth, A. *Progress in biophysics and molecular biology* **2000**, *74*, 141-173.
(53) Parikh, S. J.; Mukome, F. N.; Zhang, X. *Colloids and surfaces. B, Biointerfaces* **2014**, *119*, 38-46.
(54) Zhou, J.; Rossi, J. J. *Mol Ther Nucleic Acids* **2014**, *3*, e169.
(55) Wang, H.-Q.; Wu, Z.; Tang, L.-J.; Yu, R.-Q.; Jiang, J.-H. *Nucleic Acids Research* **2011**, *39*, e122.
(56) Deng, Q.; German, I.; Buchanan, D.; Kennedy, R. T. *Analytical Chemistry* **2001**, *73*, 5415-5421.
(57) Lee, J.-O.; So, H.-M.; Jeon, E.-K.; Chang, H.; Won, K.; Kim, Y. *Analytical and Bioanalytical Chemistry* **2008**, *390*, 1023-1032.
(58) Walter, J.-G.; Stahl, F.; Scheper, T. *Engineering in Life Sciences* **2012**, *12*, 496-506.
(59) Cheung, R. C.; Wong, J. H.; Ng, T. B. *Appl Microbiol Biotechnol* **2012**, *96*, 1411-1420.
(60) Bonanno, L. M.; Segal, E. *Nanomedicine* **2011**, *6*, 1755-1770.
(61) Li, L.-L.; Ge, P.; Selvin, P. R.; Lu, Y. *Analytical Chemistry* **2012**, *84*, 7852-7856.
(62) Huang, D.; Niu, C.; Li, Z.; Ruan, M.; Wang, X.; Zeng, G. *The Analyst* **2012**, *137*, 5607-5613.
(63) Swensen, J. S.; Xiao, Y.; Ferguson, B. S.; Lubin, A. A.; Lai, R. Y.; Heeger, A. J.; Plaxco, K. W.; Soh, H. T. *Journal of the American Chemical Society* **2009**, *131*, 4262-4266.
(64) Lonne, M.; Zhu, G. H.; Stahl, F.; Walter, J. G. In *Biosensors Based on Aptamers and Enzymes*, Gu, M. B.; Kim, H. S., Eds., 2014, pp 121-154.

For Table of Contents Only – Abstract Graphics

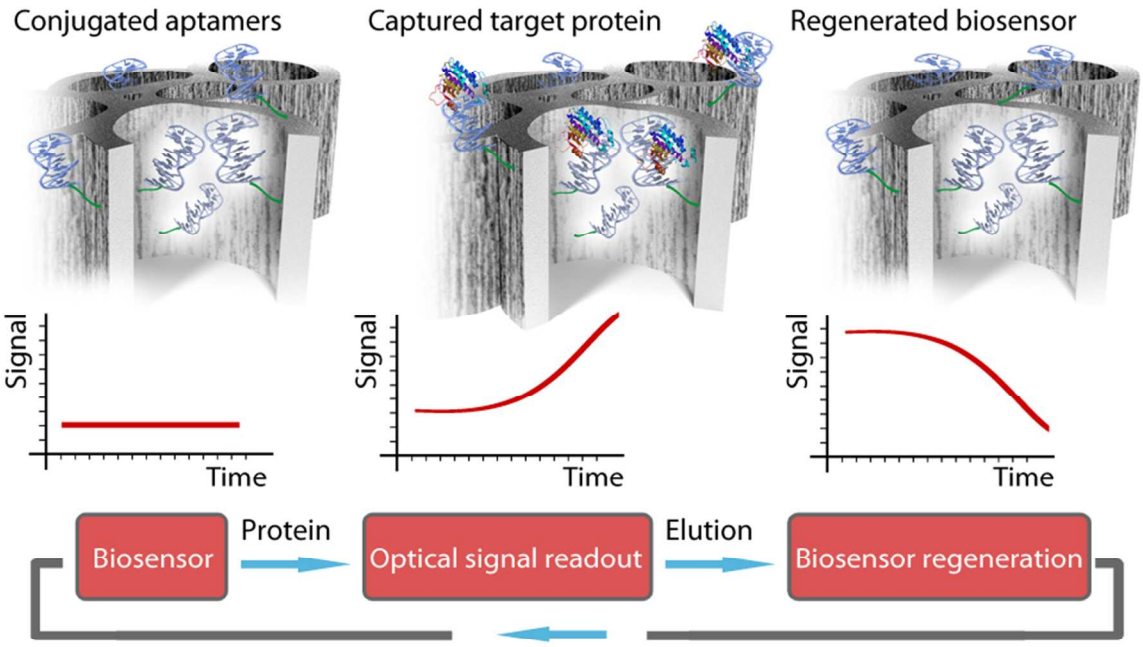
Conjugated aptamers
Captured target protein
Regenerated biosensor
Signal
Time
Signal
Time
Signal
Time
Biosensor
Protein
Optical signal readout
Elution
Biosensor regeneration

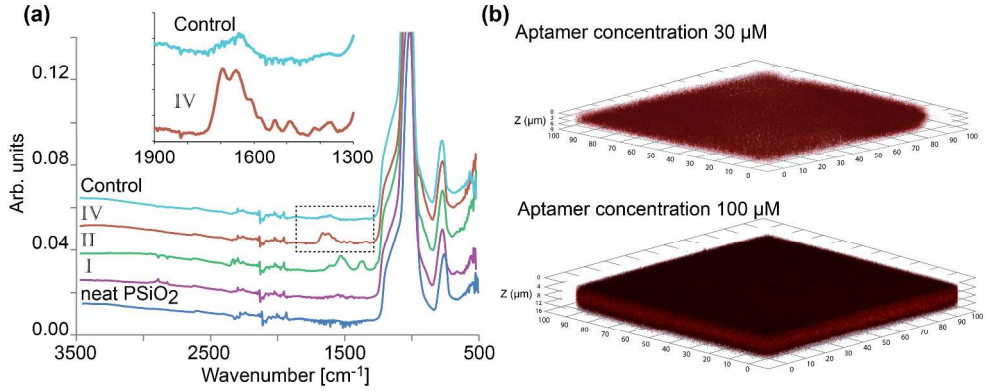

Figure 1. (a) ATR-FTIR of the different functionalization steps (illustrated in Scheme 1) followed for the preparation of aptamer-immobilized PSiO2: (I) APTES-modified surface; (II) Succinic anhydride-modified surface and (IV) 6H7-modified surface. As a control, neat PSiO2 was incubated with the 6H7 aptamer solution under similar conditions and washed with PBS. (b) Confocal microscope z-stack images of PSiO2 sensors conjugated with different aptamer-concentrations (30 µm and 100 µm of Cy5-labeled 6H7 aptamer). 1035x455mm (96 x 96 DPI)